



Dissolved valence state of iron fluorides and their effect on Ni-based alloy in FLiNaK salt



Hua Ai ^{a,b,c}, Yiyang Liu ^{a,d,1}, Miao Shen ^{a,b,c,*}, Huajian Liu ^{a,c,d}, Yanjun Chen ^{a,b,c}, Xinmei Yang ^{a,b,c,*}, Hongtao Liu ^{a,b,c}, Yuan Qian ^{a,b,c}, Jianqiang Wang ^{a,b,c}

^a Shanghai Institute of Applied Physics, Chinese Academy of Sciences, Shanghai 201800, China

^b Dalian National Laboratory for Clean Energy, Dalian 116023, China

^c Key Laboratory of Interfacial Physics and Technology, Chinese Academy of Science, Shanghai 201800, China

^d University of Chinese Academy of Sciences, Beijing 100049, China

ARTICLE INFO

Keywords:

- A. Nickel
- A. Molten salts
- B. Cyclic voltammetry
- C. Alkaline corrosion
- C. High temperature corrosion

ABSTRACT

In this study, the stable dissolved valence state of iron fluorides in molten LiF - NaF - KF (FLiNaK) salt and their effect on GH3535 alloy were systematically investigated. Results of in situ ultraviolet-visible (UV-Vis) absorption spectroscopy and electrochemical analysis indicated that Fe (II) in molten FLiNaK salt is unstable and gets converted to more stable Fe (III) through the disproportionation reaction: $3 \text{Fe (II)} = 2 \text{Fe (III)} + \text{Fe}$. Thus, the corrosion of GH3535 alloy is aggravated by the addition of iron fluorides due to the redox reaction: $\text{Fe (III)} + \text{Cr} = \text{Fe} + \text{Cr (III)}$, resulting in the formation of the Cr-depletion layer and Fe-rich layer.

1. Introduction

Molten salts have been widely used in numerous applications, such as heat transfer media for molten salt reactors (MSR), solar energy storage facilities, and hydrogen production [1–4]. Eutectic LiF - NaF - KF (FLiNaK) was proposed for use as coolant in the secondary loop of the MSR owing to its excellent chemical stability at high temperatures [5]. However, the corrosion of structural material pose a radical challenge for the application of molten fluorides [6]. The corrosion resistance of alloy elements has a tendency of Ni > Fe > Cr > Co, thus, Ni-based alloys exhibit superior corrosion resistance than Fe-based alloys. The Hastelloy N alloy (Ni-17Mo-6Cr) is successfully developed and used for MSR by Oak Ridge National Laboratory. Up to now, many literatures have reported that the corrosion of materials in molten fluorides is mainly driven by the oxidizing impurities, such as water, oxides, acid radical ions, and metal ions [7–9]. Therefore, sparging a gas mixture of H₂ and HF to react with these highly corrosive impurities is a commonly used strategy to prevent or mitigate corrosion of molten fluorides [10–12].



However, the purification treatment in the metallic containers can introduce metallic fluorides, and the corrosion of metallic materials

during the operation of MSRs also introduces metallic fluorides through Eq. (1) [12]. Therefore, it is crucial to investigate the effect of metallic fluorides on the corrosion of alloys. Studies have demonstrated that chromium fluorides [8,13,14] distinctly aggravated the corrosion of pure metal (Ni, Cr and Fe), Hastelloy N, 316 SS and SiC in molten FLiNaK salts. Researchers at the Oak Ridge National Laboratory found that both nickel and iron fluorides accelerated the corrosion of structural alloys [15–17]. Pavlik et al. [18] demonstrated that FeF₂ and FeF₃ (0.01–10 mol% in FLiNaK salt) can both significantly accelerate the corrosion of 800H. But they did not reveal the corrosion mechanism driven by metallic ions in fluorides. Our previous study [19] observed that relatively high concentration of Fe in FLiNaK salt resulted in the deposition of metallic Fe on the alloy surface. Because of the challenges of determining the specific valence state of iron in molten fluorides, the corrosion mechanism induced by iron fluorides has not been elucidated.

High-temperature ultraviolet-visible (UV-vis) absorption spectroscopy is an effective technique to detect the chemical valence state of iron fluorides in molten FLiNaK salt. The 3d-orbitals of Fe are partially filled and tend to coordinate with the ligands. The energy level of 3d-orbitals can be described by the action of the crystal field, and the d-d-orbital energy splitting depends on both the valence state of iron and the type of ligands. For instance, absorption bands for ferric nitrate in an aqueous

* Corresponding authors at: Shanghai Institute of Applied Physics, Chinese Academy of Sciences, Shanghai 201800, China

E-mail addresses: shenmiao@sinap.ac.cn (M. Shen), yangxinmei@sinap.ac.cn (X. Yang).

¹ This author contributed equally to this work.

solution are generated at ultraviolet wavelengths and begin to weaken beyond a wavelength of 550 nm [20]. By contrast, the absorption band for iron cyanide in the aqueous solution appears at 350–500 nm [21], and that for the iron divalent ion is located in the near-infrared region (>800 nm). The absorption spectra of iron ions in molten salt were mainly studied in the 1960s and 1970s. George [22] found that the absorbance peak for Fe (III) trivalent ions in LiCl - KCl salt appeared at 350–450 nm. Young et al. [23] reported that Fe (II) divalent ions in molten fluorides exhibited absorbance peaks and shoulders from 700 to 1200 nm. Therefore, the spectroscopy techniques may be useful to determine the valence state of iron ions in molten fluoride salts. Furthermore, electrochemical techniques also can be used to investigate the stable valence of electro - active species because of the quick response and in situ monitoring. Bing [1] proposed that Fe (III) trivalent ions could be converted to Fe (II) divalent ions in KCl-CaCl₂-NaCl-MgCl₂ melts by cyclic voltammetry. Our previous work also confirmed the stable existence of Cr (III) in FLiNaK salt through cyclic voltammetry and square wave voltammetry [3].

The aim of the present study was to explore the dissolution mechanism and stable valence state of iron ions in molten FLiNaK salt at 700 °C through in situ ultraviolet-visible (UV-vis) absorption spectroscopy and electrochemical techniques, which can further elucidate the corrosion mechanism of nickel-based alloy driven by iron fluorides.

2. Experimental

2.1. Materials

The eutectic FLiNaK (LiF-NaF-KF, 46.5: 11.5: 42 mol%) molten salts were supplied by Shanghai Institute of Applied Physics, Chinese Academy of Science. The major metallic impurities in this batch of salt were: Ni (90.8 ± 10.6 ppm), Fe (13.6 ± 3.7 ppm), Mo (2.5 ± 1.2 ppm), and Cr (1.7 ± 0.6 ppm), which were analysed using inductively coupled plasma optical emission spectroscopy (ICP - OES). Various quantities of FeF₂ (Alfa-011486, 98%) and FeF₃ (Aldrich-288659, 98%) were added to FLiNaK salt to prepare 100–2500 µg/Kg salt samples. The test alloy used in this study was nickel-based GH 3535 alloy, which possesses comparable composition and performance with that of Hastelloy-N alloy [24]. The chemical composition of GH 3535 alloy was listed in Table 1. The samples were cut into 15 mm × 10 mm × 2 mm sheets.

2.2. UV-Vis and electrochemical analysis

The stable valence state of iron fluorides in molten FLiNaK salt was analysed using high-temperature in situ UV-vis absorption spectroscopy [25] and electrochemical techniques. Approximately 3.0 g of FLiNaK - FeF₂ (2500 ppm) salt was transferred to a quartz sample cell (light path, 10 mm), which was placed in an electric furnace and protected by argon atmosphere. A light beam from a deuterium tungsten lamp (ideaoptics, iDH2000) was guided through the middle of the sample cell by a set of optical lenses, and the transmitted light was focused onto a spectrometer (Ocean Optics Co., QE Pro 65) to obtain the absorption spectra.

Electrochemical investigation was performed using the three-electrode system, and the schematic has been reported in the previous work [26]. A graphite rod (6.0 mm in diameter) with a large surface area served as the auxiliary electrode. Ni/NiF₂ was used as the reference electrode, which was prepared by encapsulating FLiNaK-NiF₂ (5 mol%) powder and nickel wire in a thin-wall boron nitride sleeve [27]. Tungsten wire (Φ 1 mm) was used as the working electrode, and its effective area was determined by its immersion depth in salts. All electrochemical

tests were conducted inside a high-purity argon-protected glove box, with water and oxygen contents less than 10 ppm. Prior to the experiment, all electrodes were polished with abrasive paper and cleaned with ethanol. Cyclic voltammetry (CV) and square wave voltammetry (SWV) were conducted on a tungsten working electrode to explore the stable valence state of iron ions in molten FLiNaK salt. The sweep rate of CV experiment was selected as 0.1 V/s, and the scanning frequencies of SWV were in the range of 10–50 Hz. For SWV, the step potential was −5 mV, and the amplitude was −20 mV. The conditioning potential was zero for CV or SWV, and the conditioning time was 5 s. All the electrochemical experiments were conducted at a computer-controlled AUTOLAB digital electrochemical workstation (PGSTAT 302N, Metrohm AutoLab Co., Ltd) at 700 °C, and data were processed with Nova software.

2.3. Corrosion experiments and characterizations

The static immersion tests were conducted in the isothermal capsules at 700 °C. Because the corrosion process driven by corrosive impurities primarily proceeded within 400 h, the immersion time was selected as 400 h [28–30]. The experimental details have been described in previous studies [19,31,32]. Three parallel samples were placed in each crucible, and then loaded with 250 g fluoride salt. One crucible was filled with 250 g FLiNaK salts without addition of iron fluorides, the others were FLiNaK with FeFe₂ or FeF₃ in the range from 60 ppm to 600 ppm [12]. The chemical composition of test salts after corrosion were analysed by ICP-OES. The weight changes per area were calculated by measuring the sample mass and dimension before and after immersion tests in Eq. 2.

$$\Delta M = \frac{m_0 - m_1}{S} \quad (2)$$

where ΔM is the weight change of per area (mg/cm^2), m_0 is the samples mass before corrosion (mg), m_1 is sample mass after corrosion (mg) and S is the surface area of samples (cm^2).

The microstructures and elemental distribution of the corroded samples were analysed through a scanning electron microscope (SEM, LEO 1530VP) equipped with an energy dispersive X-ray spectrometer (EDS). The crystal phases of molten salts were characterized through X-ray diffraction (XRD: Bruker D8 Advance) with a Cu K_{α1} radiation source ($\lambda = 1.5406 \text{ \AA}$). The continuous θ - 2θ scans mode at a tube power of 40 kV/40 mA in a range of 10–90° (2θ) with step = 0.02° (2θ) and 0.15 s per step.

3. Results and discussion

3.1. The stable valence state of iron ions in molten FLiNaK salt

3.1.1. UV-Vis absorption spectroscopy analysis

Fig. 1 displays the UV-vis absorption spectra of FLiNaK - FeF₂ (2500 ppm) salt from 0 to 600 min after heating at 700 °C. No peaks initially appeared at 350–970 nm in FLiNaK salt (Fig. 1 line 1). After 2500 ppm of FeF₂ was added to the salt and maintained for 10 min, two absorption peaks at 375–600 nm and 700–970 nm, were observed (Fig. 1 line 2). Since the FeF₂ and FeF₃ performed as Lewis acids [33], they would interact with the Lewis base F[−] (LiF/NaF/KF) to form complexes, such as [FeF₄]^{2−}, [FeF₄][−] and [FeF₆]^{3−} [33,34]. Hence, the absorption peak at 375–600 nm can be assigned to Fe (III) trivalent ions, which was in agreement with George's results obtained for LiCl - KCl molten salts [22]. The absorption peak at 700–970 nm can be assigned to Fe (II) divalent ions owing to the dissolution of FeF₂ in the form of [FeF₄]^{2−} in molten FLiNaK salt [23]. These results indicate that the dissolution of FeF₂ and its conversion to Fe (III) occur simultaneously after FeF₂ was added to FLiNaK salt. At 30 min, the absorbance of Fe (III) and Fe (II) had increased to 0.07 and 0.13, respectively (Fig. 1 line 3). At 90 and 180 min, the absorbance of Fe (III) had increased to 0.14 and

Table 1
Chemical composition of GH 3535 samples (wt%).

Ni	Mo	Cr	Fe	Si	Ti	C
Base	17.34	7.01	3.92	0.45	0.002	0.055

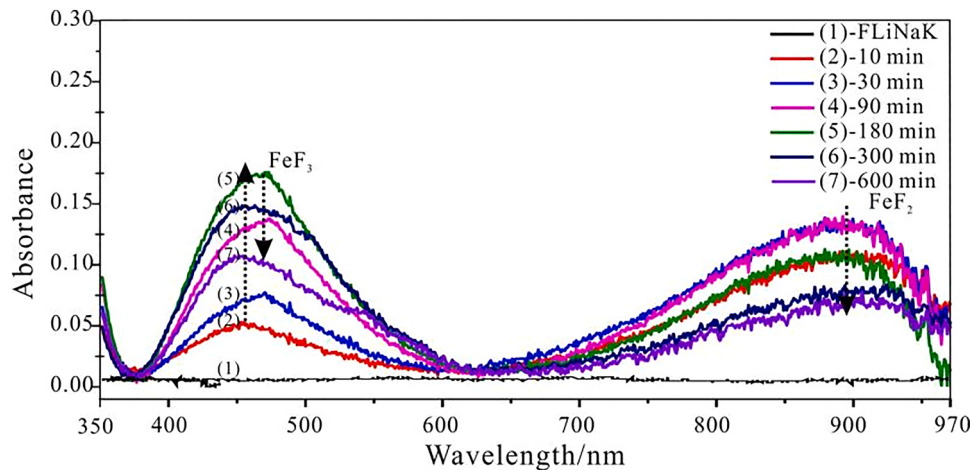


Fig. 1. The UV–Vis absorption spectra of molten FLiNaK - FeF₂ (2500 ppm) salt system as a function of dissolution time at 700 °C.

0.17, respectively (Fig. 1 line 4 and 5), and at 300 and 600 min, it gradually decreased to 0.15 and 0.10, respectively. However, the absorbance of Fe (II) started to decrease from 90 to 600 min.

Based on the Beer–Lambert law [35], the absorbance of Fe (III) or Fe (II) in molten fluorides is proportional to its concentration, as shown in Eq. (3).

$$A = \varepsilon bc \quad (3)$$

Where A is the absorbance, ε is the absorptivity, g/(g·cm) (here it is a constant), b is the distance of the light path, cm (here, 1 cm) and c is the concentration of Fe (III) or Fe (II) in the molten salts, g/g.

Based on Eq. (3), we deduce that the concentration of Fe (II) increases as time increases from 0 to 30 min, and then begins to decrease from 90 to 600 min. This result indicates that the dissolution rate of FeF₂ to [FeF₄]²⁻ (Eq. 4) is greater than the rate of conversion of [FeF₄]²⁻ to Fe (III) during the initial 30 min, thus, the Fe (II) absorbance peak gradually increased. When the dissolution from FeF₂ to [FeF₄]²⁻ was completed, the conversion of [FeF₄]²⁻ to Fe (III) caused a decrease in the Fe (II) absorbance peak.

The concentration of Fe (III) increased as time increased from 0 to 180 min and then decreased at 300 and 600 min. Early studies have reported that Fe (III) tends to combine with F⁻ to form a complex, [FeF₆]³⁻, which is an octahedral crystal field, and its d5 orbital has a t2g3eg2 distribution with no d-d orbital transition. Hence, no absorption peak for [FeF₆]³⁻ was observed in the visible region [36] and the additive F⁻ is usually used to shield Fe (III) impurity in the aqueous solution [22]. In addition to [FeF₆]³⁻, Fe (III) also exists in the form of [FeF₄]⁻, but this species is less stable than [FeF₆]³⁻ [37,38]. Thus, we can reasonably deduce that the absorption peak at 400–550 nm can be attributed to [FeF₄]⁻, the concentration of which increased as time increased from 0 to

180 min because of the conversion of [FeF₄]²⁻ to [FeF₄]⁻ (Eq. 5). However, [FeF₄]⁻ could further combine with F⁻ to form the more stable [FeF₆]³⁻ ions (Eq. 6), which has no absorption peak at the UV-visible band [29], resulting in a decrease in the concentration of [FeF₄]⁻ in 300–600 min. After UV–vis absorption spectra experiments, the XRD pattern of solid power salts revealed the presence of Na₃FeF₆, K₃FeF₆, and metallic Fe in FLiNaK - FeF₂ salt, as shown in Fig. 2. The K₃FeF₆/-Na₃FeF₆ complexes were formed by the reaction of [FeF₆]³⁻ and K⁺/Na⁺ (Eq. 8), which deposited from molten salt as the corrosion products [39]. The existence of Fe was caused by the nonelectrical transfer in molten salts reported by Ozeryanaya [40]. Therefore, the formation of Na₃FeF₆, K₃FeF₆, and Fe was related to the disproportionation reaction in FLiNaK salt, as shown in Eq. (7), suggesting that FeF₂ additives was unstable in molten FLiNaK salt. Actually, early ORNL researches [3,41] have proved that FLiNaK with plenty of free F⁻ is a strongly basic solvent, which tends to stabilize the M(III) (M= Cr/Fe) oxidation state and provides a stronger corrosion driving force due to the variation of oxidation states [Cr(II/III), Fe(II/III)].

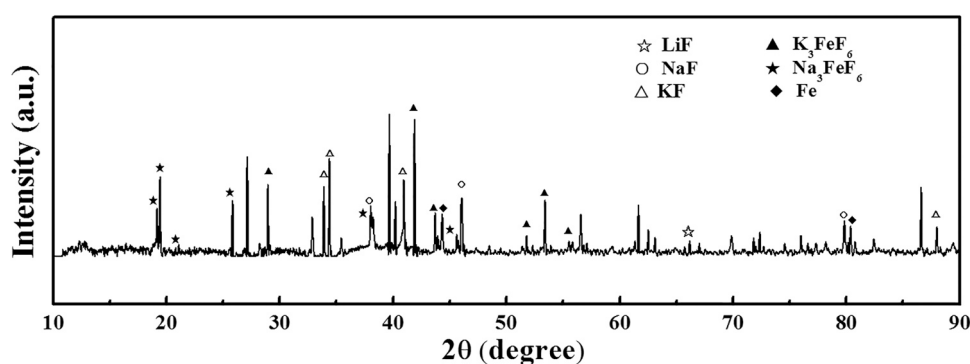
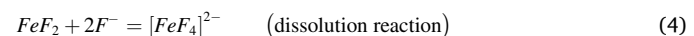


Fig. 2. XRD pattern of FLiNaK - FeF₂ salt.

3.1.2. CV and SWV analysis

To further validate the speculation acquired by UV–Vis absorption spectroscopy, the electrochemical behaviour of iron ions in FLiNaK was studied through cyclic CV and SWV owing to their high validity for the investigation of stable electro-active species [42,43]. Fig. 3 presents the typical cyclic voltammetry of the FLiNaK - FeF₂ (1000 ppm) system recorded on a tungsten electrode at 0.1 V/s, where three couples of cathodic/anodic signals A/A', B/B', and D/D' are observed. The D/D' signal corresponds to the reduction of one melt component. According to heat of formation of fluorides obtained from the studies of Baes [44] and Durán-Klie [45], we can assume that signal D corresponds to the electrodeposition of potassium, whereas the oxidation signal D' should be associated with the dissolution of potassium. Accordingly, the other two reduction peaks A and B, exhibited at −0.03 and −0.41 V (vs. Ni/NiF₂), and their corresponding oxidation peaks, A' and B', should be related to FeF₂ addition.

To explore the corresponding reactions at peaks A and B, SWV was further employed to determine the number of transferred electrons. Two reduction peaks, A and B, were detected at −0.11 and −0.48 V (vs. Ni/NiF₂), respectively, which was consistent with the results obtained from CV. The number of transferred electrons for peaks A and B can be calculated using Eq. (9). The result is theoretically valid for reversible systems and can be extended to other systems if the criterion of linearity between the peak intensity and the square root of the frequency signal is satisfied [43].

$$W_{1/2} = 3.52 \frac{RT}{nF} \quad (9)$$

where $W_{1/2}$ is the half-width of the peak, R is the gas constant, 8.314 J/(mol K), T is temperature in K, n is the number of electrons involved in the reaction, and F is Faraday's constant, 96,485 C/mol.

Obviously, the current intensity of peaks A and B is linear, with the square root of the frequency in the range of 10–50 Hz (Fig. 4b and c). The number of electrons transferred for peaks A and B calculated by Eq. (9), is approximately 1 and 2, respectively. Thus, peak A at −0.11 V (vs. Ni/NiF₂) and peak B at −0.48 V (vs. Ni/NiF₂) should correspond to the reduction of Fe (III)/Fe (II) and Fe (II)/Fe, respectively, as shown in Table 2. The presence of Fe (III) / Fe (II) proves that FeF₂ is unstable and gets converted to Fe (III) in molten FLiNaK salt. These results are consistent with those obtained by UV-vis analysis. A similar phenomenon was observed for CrF₂ in molten FLiNaK salt [14].

3.1.3. Conversion rate of Fe (II) to Fe (III) in FLiNaK salt

The results of the UV-vis and electrochemical analyses indicate that

FeF₂ is unstable in molten FLiNaK salt, and it converts to Fe (III) through the disproportionation reaction (Eq. 7). To confirm the conversion rate, the relation between Fe (III)/Fe (II) current densities and the Fe (III) concentrations within 1000 ppm was established through CV analysis. At a temperature of 700 °C, the peak current density of peak A for Fe (III)/Fe (II) increased with the concentration of Fe (III) within 1000 ppm, and a linear relationship was observed at a scan rate of 0.1 V/s (Fig. 5). The equation of this straight line is as follows:

$$\delta i p_A \left(\frac{mA^2}{cm} \right) = -0.00448 [Fe(III)] (ppm) \quad (10)$$

Based on the CV result shown in Fig. 3, i_p assigned to the reduction current density of Fe (III)/Fe (II) eventually remained at −2.45 mA/cm²; thus, the concentration of Fe (III) was 545 ppm as calculated using Eq. (10). Because Fe (III) is generated from a disproportionation reaction (Eq. 7), we can deduce that 819 ppm Fe (II) was converted to 545 ppm Fe (III). Therefore, the conversion ratio of Fe (II) to Fe (III) in molten FLiNaK salt was approximately 81.9% considering the initial concentration of FeF₂ was 1000 ppm.

3.2. The corrosivity of iron fluorides on GH 3535 alloy in molten FLiNaK salt

Based on the analysis in Section 3.1, the stable valence state of iron fluorides in FLiNaK salt was thoroughly investigated, which provided insights into their corrosivity on structural alloys.

3.2.1. The corrosion of GH 3535 alloy in FLiNaK - FeF₂ salt

The change in sample weights after the corrosion in molten FLiNaK salt with different contents of FeF₂ at 700 °C for 400 h was shown in Fig. 6, where plus sign (+) denotes weight loss and the minus sign (−) indicates weight gain after corrosion. The weight loss of GH3535 samples was 0.55 mg/cm² in FLiNaK salts without FeF₂, which can be attributed to the dissolution of elements from bulk samples into salts. After corroded in FLiNaK salt with 60 ppm FeF₂, the weight loss of the samples was descended to 0.48 mg/cm². Then, the weight loss of GH3535 sample gradually decreased to 0.12 mg/cm² in FLiNaK salt with 240 ppm FeF₂. When the FeF₂ content was further increased to 600 ppm, the weight gain of the GH3535 samples was 1.574 mg/cm². Given the sample mass change from weight loss to weight gain, it can be speculated that FeF₂ addition could change the corrosion mechanism or corrosion products of GH 3535 alloy in molten FLiNaK salt.

Fig. 7 presents the surface scanning electron microscopy (SEM) and

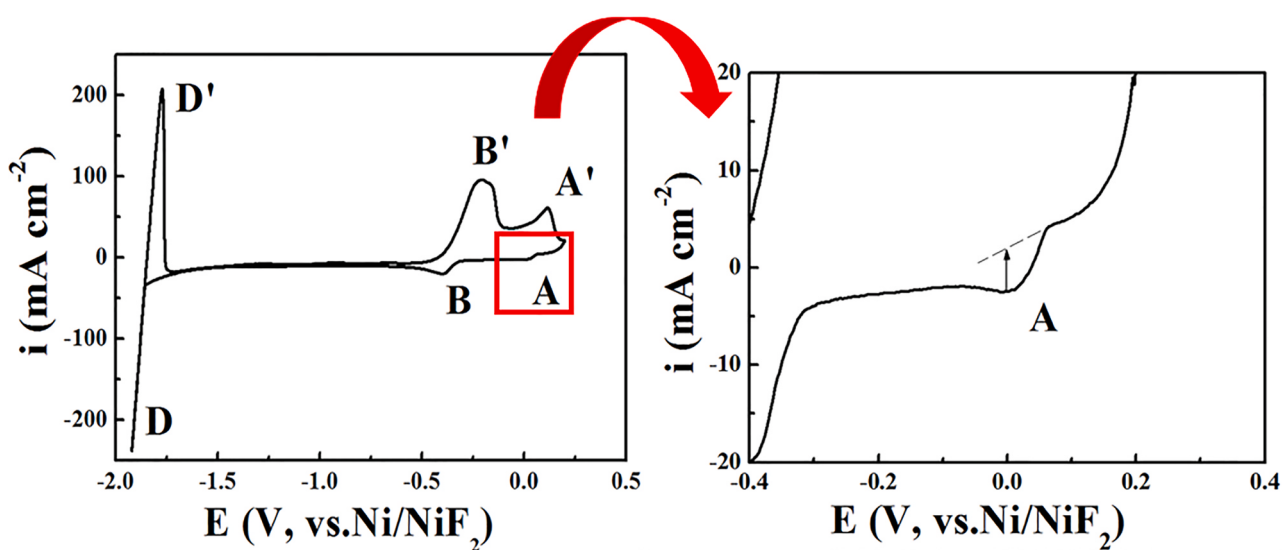


Fig. 3. Cyclic voltammetry curve of FLiNaK - FeF₂ (1000 ppm) system at 700 °C and the scan rate of 0.1 V/s on a W electrode.

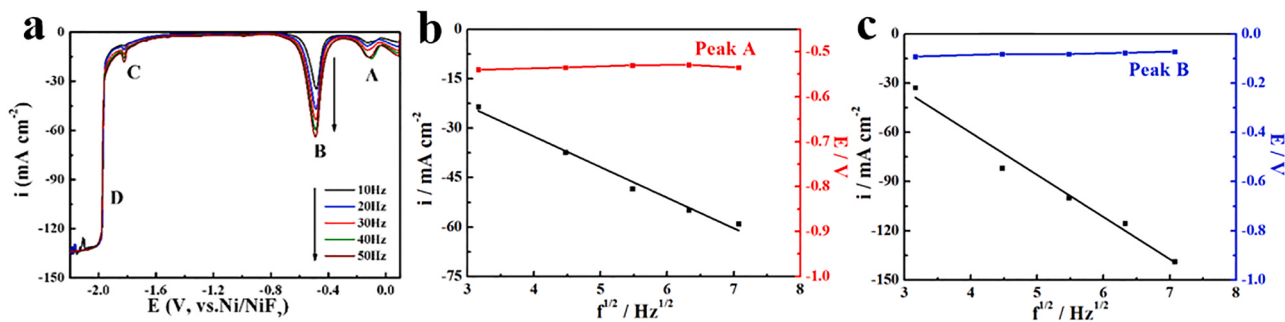


Fig. 4. (a) Square wave voltammetry of FLiNaK - FeF₂ (1000 ppm) obtained on a tungsten electrode at 700 °C and different scanning frequencies. Plots of peak current density and peak potential vs. the square root of the frequency for cathodic peak A (b) and peak B (c).

Table 2

Reduction potentials and electron-transfer numbers for peak A and B.

Reduction Peaks	A	B
Reduction potential vs. Ni/NiF ₂	-0.11 V	-0.48 V
W _{1/2}	232 mV	133 mV
Electron-transfer numbers	1.14	1.99
Corresponding reaction	Fe (III) + e = Fe (II)	Fe (II) + 2e = Fe

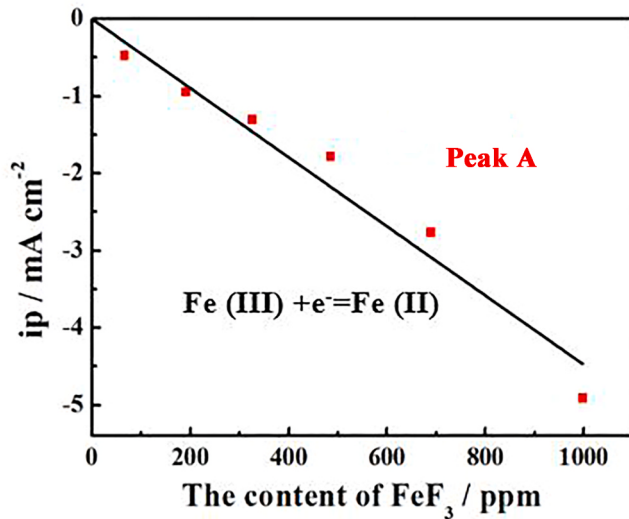


Fig. 5. Linear relationship between the peak current density and Fe(III) concentration in FLiNaK salt with scan rate of 0.1 V/s for cathodic peaks A: Fe(III) + e⁻ = Fe(II).

energy-dispersive spectroscopy (EDS) images of GH3535 alloy after corrosion in molten FLiNaK salt with and without FeF₂. After corrosion in molten FLiNaK salt without FeF₂ (Fig. 7a), numerous corrosion voids were observed on the surface of GH3535 samples, resulting from the depletion of alloy ingredients. After corrosion in molten FLiNaK salt with 60 ppm FeF₂ (Fig. 7b), corrosion voids with a reduced pore density were observed on the surface of alloy. After corrosion in molten FLiNaK salt with 600 ppm FeF₂, the sample surface was covered by a layer of uniform corrosion products with a typical crystalline structure (Fig. 7c). The EDS results revealed that FeF₂ addition in molten FLiNaK salt caused the relative decrease in the content of Ni, Cr and Mo on the GH3535 alloy surface, whereas the content of Fe increased from 4.24 wt% to 30.48 wt%. It is speculated that iron fluorides in molten FLiNaK salt may drive the corrosion of Cr and Mo. Table 3 shows the concentrations of Ni, Mo, Cr and Fe in salts analyzed by ICP-OES. Results show that the concentrations of Ni, Cr and Mo evidently increase further indicating that iron fluorides in molten FLiNaK salt drive the diffusion of Ni, Cr and

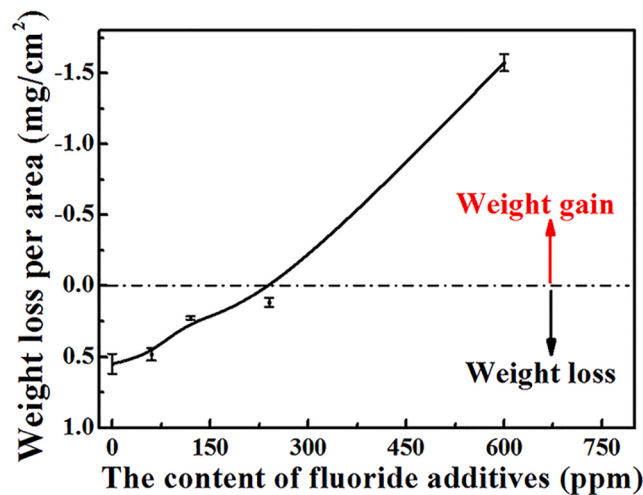


Fig. 6. Weight change of the GH3535 alloy after corrosion as a function of the content of FeF₂ in molten FLiNaK salt.

Mo from alloy matrix into the molten salt. Since the results of the UV-vis and electrochemical analyses indicate that FeF₂ in molten FLiNaK salt converts to Fe (III) through the disproportionation reaction, it is possible for FeF₃ to react with Ni, Cr and Mo, as shown in Table 4. These reactions lead to the concentration of Fe distinctly decrease by around 27% from above 600–436 ppm, resulting in the formation of metallic Fe [19,30], which may be the main reason for the weight gain of GH3535 samples in Fig. 6.

The thickness of the Cr-depletion layer is an important index to evaluate the corrosion degree of Cr-containing alloys in molten fluoride salts [19,46–48]. The cross-sectional images and the distribution of elements in corroded GH3535 alloy samples are shown in Fig. 8. The content of element Cr on the surface was obviously lower than that in the matrix after corrosion in FLiNaK salt, and the depletion layer was approximately $10 \pm 0.5 \mu\text{m}$ (Fig. 8d1). After corrosion in FLiNaK salt with 60 ppm FeF₂, the thickness of the Cr-depletion layer increased to approximately $12 \pm 0.5 \mu\text{m}$ (Fig. 8e1). Moreover, the Fe content near the alloy surface slightly increased (Fig. 8e2). After corrosion in molten FLiNaK salt with 600 ppm FeF₂, the Cr-depletion layer was approximately $13 \pm 0.5 \mu\text{m}$ (Fig. 8f1) with more Cr atoms depleted from the alloy matrix as compared to that in Fig. 8e1. The Fe content adjacent to the alloy surface significantly increased (Fig. 8f2), resulting in the formation of a Fe-rich layer of approximately $14 \pm 0.5 \mu\text{m}$. Moreover, the depletion of Ni and Mo can also be observed in Cr-depletion and Fe-rich layer (Fig. 8f). Considering most Fe (II) in molten FLiNaK salt were converted to Fe (III) as confirmed by UV-vis and CV/SWV, the reaction of Fe (III) ions with Cr, Ni and Mo in the alloy led to the depletion of Ni, Cr and Mo, and the formation of Fe-rich layer as shown in Table 4. These

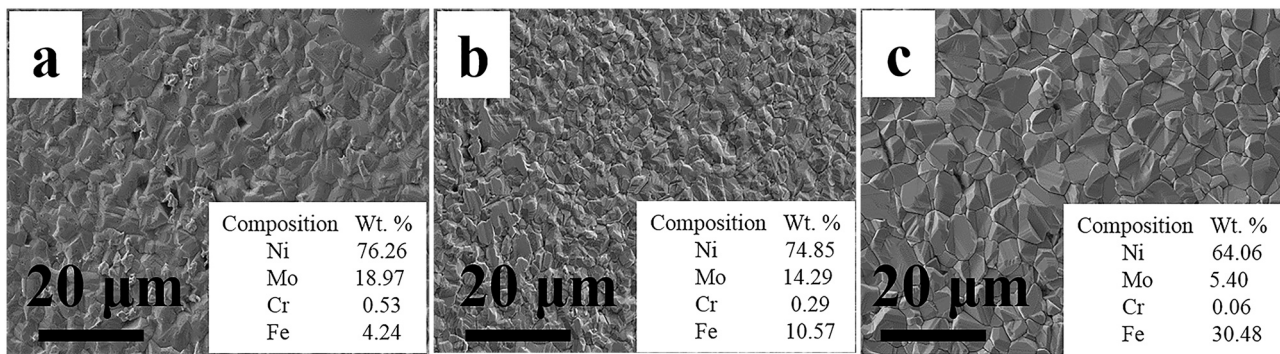


Fig. 7. Surface images and composition of GH 3535 alloy after corrosion in molten FLiNaK salt with (a) 0 ppm (b) 60 ppm and (c) 600 ppm FeF₂.

Table 3

The concentrations of Mo, Cr and Fe in FLiNaK salts before and after corrosion (unit: µg/g).

Molten Salts	Ni	Mo	Cr	Fe
As received FLiNaK salt	90.9 ± 10.6	2.5 ± 1.2	1.7 ± 0.6	13.6 ± 3.7
FLiNaK after corrosion	67.2 ± 5.8	6.3 ± 0.6	24.4 ± 1.3	12.1 ± 1.8
FLiNaK - FeF ₂ (600 ppm) after corrosion	109.2 ± 8.3	25.3 ± 1.6	32.6 ± 2.1	436.2 ± 10.7

Table 4

Possible reactions of FeF₃ with metallic elements at 700 °C.

Reactions	Δ _r G _{700 °C} (kJ / mol)
FeF ₃ + Cr = Fe + CrF ₃	-149.809
FeF ₃ + 1.5 Ni = 1.5 NiF ₂ + FeF ₂	-73.704
3FeF ₃ + Mo = 3FeF ₂ + MoF ₃	-41.343

results are consistent with those obtained from the salt compositions analysed by ICP-OES in Table 3.

3.2.2. The corrosion of GH 3535 alloy in FLiNaK - FeF₃ salt

To verify whether the reaction of Fe (III) ions and Cr in GH3535 alloy leads to the corrosion of the alloy, the alloy was subjected to static corrosion tests in FLiNaK salt with 600 ppm FeF₃. Fig. 9a shows the surface SEM image of GH3535 alloy after undergoing corrosion in molten FLiNaK - FeF₃ salt. Obviously, the sample surface was uniformly covered with corrosion products, similar to that shown in Fig. 7c. The Cr-depletion layer was approximately 13 ± 0.5 µm thick (Fig. 9c), and the Fe content in the Cr-depletion layer was higher than that in the matrix. These results are consistent with those obtained for FLiNaK - FeF₂ (600 ppm) system. Furthermore, in our previous research, Fe deposited on the alloy surface was confirmed to be zero valent metal state [19]. These results further indicate that iron fluorides in FLiNaK salts aggravate the depletion of Ni, Cr and Mo, resulting in the severe corrosion of GH 3535 alloy.

3.2.3. Corrosion process analysis

The corrosion of alloy structural materials in molten fluoride salts is mainly controlled by the thermodynamic driving force of alloying constituents to form metal fluorides. Given the Gibbs free energy of molten salt constituents (LiF, NaF, KF) are more negative than those of metallic fluorides (Table 5), pure alkali fluorides cannot cause the corrosion of alloys. However, the presence of oxidizing impurities, such as FeF₃/FeF₂, CrF₃, H₂O/HF and SO₄²⁻ in salts, can cause the corrosion of alloys owing to the negative values of Δ_rG° at 700 °C. In this work, the FLiNaK salts were purified to remove most impurities, such as water and acid radical ions. But slight corrosion of GH3535 alloy can still be

detected in the purified FLiNaK salt (Figs. 7a, Fig. 8a and d). As the most vulnerable element in GH3535 alloy, Cr atoms tend to react with oxidizing impurities and dissolve into molten salts, resulting in the formation of Cr - depletion layer [46,49]. As shown in Table 3 the concentration of Ni is up to 90 ppm in the original FLiNaK salt, it should be the oxidizing impurities to cause the depletion of Cr from GH3535 alloy into the molten fluorides.

In the system of molten FLiNaK salt with 600 ppm iron fluorides, the results of UV - Vis absorption spectroscopy and electrochemical (CV/ SWV) analysis show that most iron fluorides would exist in the valence state Fe (III). Therefore, the total corrosion of GH3535 alloy in molten FLiNaK salts with iron fluorides occurs as follows:

- (1) The redox reactions of alloy elements (mainly Cr) and Fe (III) (Table 4) are the main cause of GH3535 corrosion in FLiNaK salt with high iron ions. These elements dissolve into molten salts, resulting in the retention of some vacancies in the Cr-depletion layer.



- (2) A mass of metallic Fe atoms accumulate on the alloy surface and diffuse into the alloy bulk to fill in the vacancies, resulting in the formation of Fe - rich layer.

The weight changes in GH3535 alloy (Fig. 6) are categorized into two parts. The first part is the weight loss caused by the dissolution of alloy elements (mainly Cr) from the matrix into the salts and denoted by ΔM_{loss}. The second part is the weight gain due to the deposition of metallic Fe atoms on the alloy surface and denoted by ΔM_{gain}. The total mass change (ΔM) is the algebraic sum of these two parts, as expressed in Eq. 12. For the GH3535 alloy corrosion in molten FLiNaK salt without iron fluorides, the diffusion of Cr is the main reason underlying the weight changes, and ΔM ≈ ΔM_{loss}. When corrosion in FLiNaK salts with iron fluorides, the part of weight loss (ΔM_{loss}) can be caused by the dissolution of Cr, Mo and Ni, but the depletion of Cr is the most significant (Fig. 8e). The part of weight gain ΔM_{gain} increases with the increasing of iron fluorides, and the total mass changes (ΔM) has changed into weigh gain of 1.574 mg/cm² when corroded in FLiNaK salt with 600 ppm iron fluorides. According to Table 4, the dissolution of 1 ppm (4.8×10^{-6} mol) Cr can result in the formation of 1.07 ppm Fe resulting in the weight gain of alloy samples.

$$\Delta M = \Delta M_{loss} + \Delta M_{gain}, \text{ where } \Delta M_{loss} > 0, \Delta M_{gain} < 0 \quad (12)$$

At the macroscopic scale, the diffusion layer of Cr is approximate to the thickness of the Cr-depletion layer. Thus, based on Fick's law of diffusion, the depth of Cr-depletion layer can be used to calculate the diffusion coefficient of Cr in the alloy, as shown in Eq. (12) [50]:

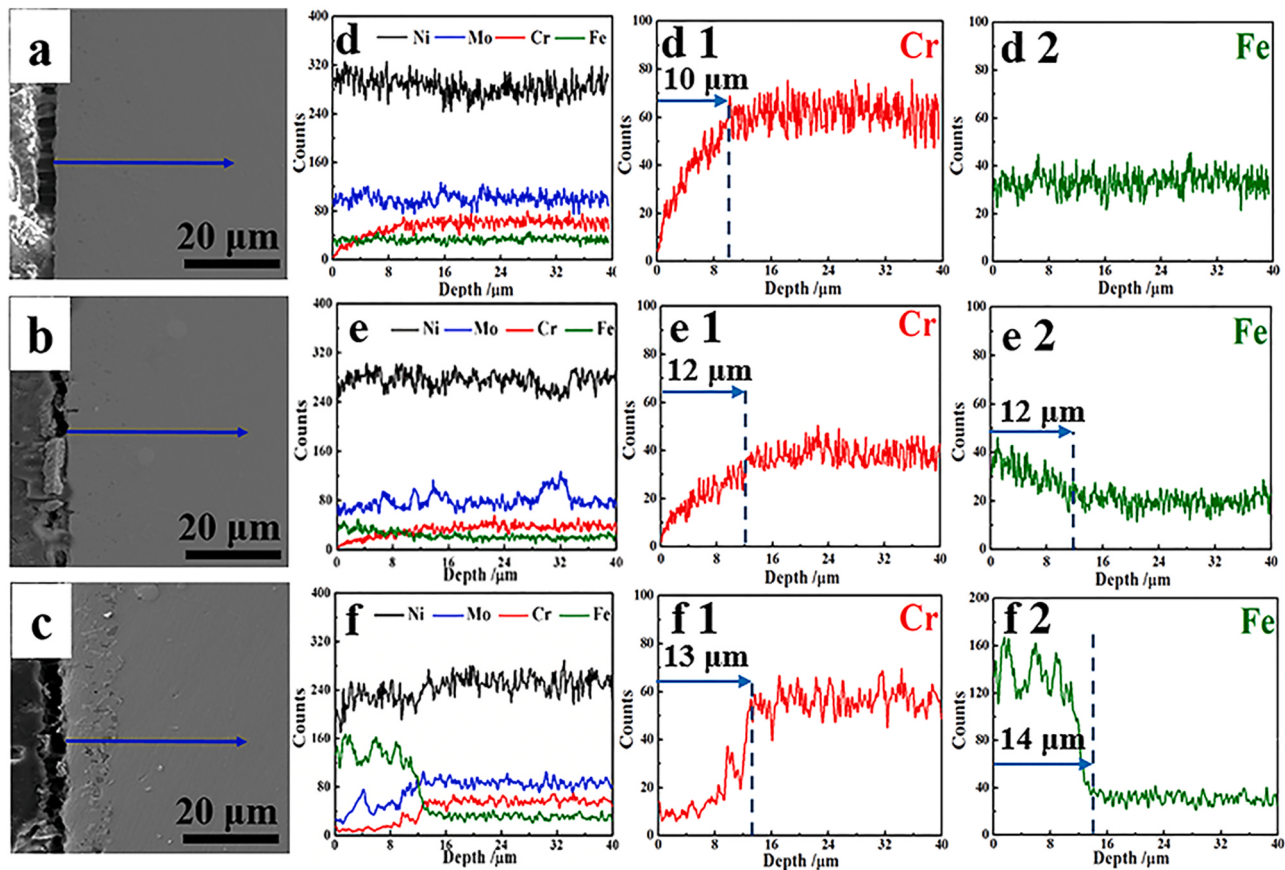


Fig. 8. Cross-sectional SEM images and line-scanning EDS spectra of GH3535 alloy after corrosion in molten FLiNaK salt with (a, d, d1, d2) 0 ppm (b, e, e1, e2) 60 ppm and (c, f, f1, f2) 600 ppm FeF₂.

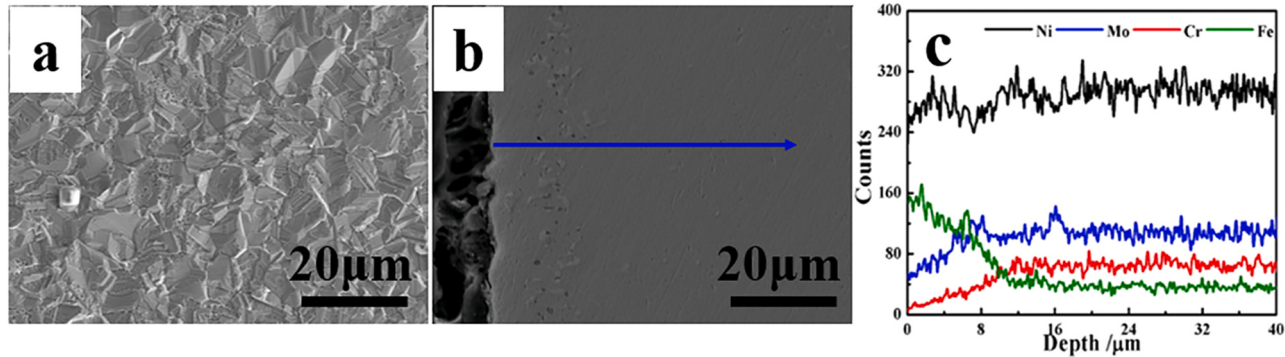


Fig. 9. SEM images and EDS spectra of GH 3535 alloy after corrosion in molten FLiNaK salt with 600 ppm FeF₃ (a) surface, (b) cross section and (c) line-scanning EDS spectra at 700 °C for 400 h.

$$x = \sqrt{2D_{\text{eff}}t} \quad (13)$$

Where x is the diffusion distance, which is approximate to the thickness of the Cr-depletion layer, m; D_{eff} is the effective diffusion coefficient of Cr in the alloy, m²/s; and t is the immersion time for corrosion, s. For GH3535 alloy in molten FLiNaK salt, the thickness of Cr-depletion layer is approximate to 10 μm, and the effective diffusion coefficient of Cr in the nickel-based alloy ($D_{\text{Cr-eff}}$) is calculated to be 3.4×10^{-17} m² s⁻¹, which is considerably lower than that of Cr ions diffusion in molten FLiNaK salt ($D_{\text{in FLiNaK}} = 2.9 \pm 0.8 \times 10^{-10}$ m² s⁻¹ at 700 °C [51]). Therefore, the corrosion rate of GH 3535 alloy is mainly determined by the diffusion rate of Cr in the alloy bulk.

When 600 ppm iron fluorides (including FeF₂ and FeF₃) were added

to FLiNaK salt, the Cr-depletion layer is approximately 13 μm thick, and $D_{\text{Cr-eff}}$ was calculated as 5.8×10^{-17} m² s⁻¹ by Eq. 12. The diffusion rate of Cr was distinctly increased by 70% in the presence of iron fluorides, indicating that the effective diffusion rate of Cr in alloy bulk is accelerated by the high concentration of iron fluorides [30] due to the redox reaction between Cr atoms and iron fluorides in molten FLiNaK salt.

4. Conclusions

The stable valence state of iron fluorides and their effect on GH3535 alloy in FLiNaK salt was systematically investigated in this study through in situ UV-vis absorption spectroscopy and electrochemical analysis. The UV-vis absorption spectroscopy results revealed that FeF₂

Table 5

Gibbs free energies of possible reactions at 700 °C calculated by HSC 6.0 software.

Reactions	$\Delta_r G_{700\text{ }^\circ\text{C}}$ (kJ/mol)
(1) $2\text{Li} + \text{F}_2(\text{g}) = 2\text{LiF}$	-1045.405
(2) $2\text{Na} + \text{F}_2(\text{g}) = 2\text{NaF}$	-950.083
(3) $2\text{K} + \text{F}_2(\text{g}) = 2\text{KF}$	-938.827
(4) $\text{Ni} + \text{F}_2(\text{g}) = \text{NiF}_2$	-505.488
(5) $2/3\text{Fe} + \text{F}_2(\text{g}) = 2/3\text{FeF}_3$	-526.017
(6) $2/3\text{Cr} + \text{F}_2(\text{g}) = 2/3\text{CrF}_3$	-625.890
(7) $\text{FeF}_3 + \text{Cr} = \text{CrF}_3 + \text{Fe}$	-149.809
(8) $2\text{FeF}_3 + \text{Fe} = 3\text{FeF}_2$	-141.351
(9) $\text{FeF}_3 + 1.5\text{Ni} = 1.5\text{NiF}_2 + \text{FeF}_2$	-73.704
(10) $3\text{FeF}_3 + \text{Mo} = \text{MoF}_3 + 3\text{FeF}_2$	-41.343
(11) $\text{FeF}_3 + 1.5\text{Ni} = 1.5\text{NiF}_2 + \text{Fe}$	30.795
(12) $\text{FeF}_3 + \text{Mo} = \text{MoF}_3 + \text{Fe}$	100.008
(13) $1.5\text{NiF}_2 + \text{Mo} = \text{MoF}_3 + 1.5\text{Ni}$	69.213
(14) $1.5\text{NiF}_2 + \text{Cr} = \text{CrF}_3 + 1.5\text{Ni}$	-180.603
(15) $1.5\text{NiF}_2 + \text{Fe} = \text{FeF}_3 + 1.5\text{Ni}$	-30.795
(16) $2\text{CrF}_3 + \text{Cr} = 3\text{CrF}_2$	-81.736
(17) $\text{CrF}_3 + 1.5\text{Ni} = 1.5\text{NiF}_2 + \text{Cr}$	180.603
(18) $\text{CrF}_3 + \text{Fe} = \text{FeF}_3 + \text{Cr}$	149.809
(19) $\text{CrF}_3 + \text{Mo} = \text{MoF}_3 + \text{Cr}$	249.816
(20) $\text{H}_2\text{O} + 2\text{F}^- = 2\text{HF} + \text{O}^{2-}$	
(21) $2\text{HF}(\text{l}) + \text{Ni} = \text{NiF}_2 + \text{H}_2(\text{g})$	-64.334
(22) $2\text{HF}(\text{l}) + \text{Fe} = \text{FeF}_2 + \text{H}_2(\text{g})$	-131.981
(23) $3\text{HF}(\text{l}) + \text{Cr} = \text{CrF}_3 + 1.5\text{H}_2(\text{g})$	-277.105
(24) $3\text{HF}(\text{l}) + \text{Fe} = \text{FeF}_3 + 1.5\text{H}_2(\text{g})$	-127.296
(25) $3\text{HF(l)} + \text{Mo} = \text{MoF}_3 + 1.5\text{H}_2(\text{g})$	-27.288
(26) $\text{Na}_2\text{SO}_4 + 2\text{Cr} = \text{S} + \text{Na}_2\text{O} + \text{Cr}_2\text{O}_3$	-157.535

initially dissolved in FLiNaK in the form of $[\text{FeF}_4]^{2-}$, which was simultaneously converted to $[\text{FeF}_4]^+$. However, due to the stronger coordination ability to free F⁻, $[\text{FeF}_4]^+$ tended to form more stable $[\text{FeF}_6]^{3-}$, which exhibits no absorption peak at the UV-vis region. Through CV and SWV analysis, the reduction peak of Fe (III) to Fe (II) was detected, which further proved that the FeF₂ additive was unstable and can be converted to Fe (III). Moreover, Na₃FeF₆, K₃FeF₆, and metallic Fe were detected in the XRD pattern of FLiNaK-FeF₂ salt, indicating the conversion of Fe (II) to Fe (III) through the disproportionation reaction: 3Fe (II) = Fe + 2 Fe (III). The corrosion of GH3535 alloy in molten FLiNaK salt was aggravated by iron fluorides (including FeF₂ and FeF₃), and the depths of the Cr-depletion and Fe-rich layers increased with the increase in the content of iron fluorides due to the redox reaction: Fe (III) + Cr = Fe + Cr (III).

Author statement

I have made substantial contributions to the conception or design of the work, or the acquisition, analysis, or interpretation of data for the work; And I have drafted the work or revised it critically for important intellectual content; And I have approved the final version to be published; And I agree to be accountable for all aspects of the work in ensuring that questions related to the accuracy or integrity of any part of the work.

All persons who have made substantial contributions to the work reported in the manuscript have been listed as the co-authors.

CRediT authorship contribution statement

Hua Ai: Investigation, Formal analysis, Visualization, Writing - Original Draft. **Yiyang Liu:** Investigation, Formal analysis. **Miao Shen and Xinmei Yang:** Conceptualization, Methodology, Writing - Original Draft, Funding acquisition. **Huajian Liu and Yanjun Chen:** Investigation, Formal analysis, **Hongtao Liu, Yuan Qian and Jianqiang Wang:** Validation, Resource, Project administration, Funding acquisition.

Declaration of Competing Interest

The authors declare that they have no known competing financial interests or personal relationships that could have appeared to influence the work reported in this paper.

Data availability

All data included in this study are available upon request by contact with the corresponding author.

Acknowledgements

This work was supported by National Science Foundation of Shanghai (Grant No. 21ZR1476200, 19ZR1468300, 17ZR1436600); the National Science Foundation of China (Grant No. 11675246, Grant No. 51801228); and the “Transformational Technologies for Clean Energy and Demonstration”, Strategic Priority Research Program of the Chinese Academy of Sciences (Grant No. XDA 21000000).

References

- [1] H. Boussier, S. Delpach, V. Ghetta, D. Heuer, D.E. Holcomb, V. Ignatiev, E. Merle-Lucotte, J. Serp, The Molten Salt Reactor in Generation IV: Overview and Perspectives, In: Proceedings of the Generation 4 International Forum Symposium, 2012.
- [2] M.H. Jiang, H. Xu, Z. Dai, Advanced fission energy program—TMSR nuclear energy system, Proc. Chin. Acad. Sci. 27 (2012) 366–374.
- [3] D.F. Williams, K.T. Clarno Assessment of Candidate Molten Salt Coolants for the Advanced High-Temperature React. (AHTR), ORNL-TM 2006/12 2006 1 69.
- [4] M. Liu, N. Tay, S. Bell, M. Belusko, R. Jacob, G. Will, W. Saman, F. Bruno, Review on concentrating solar power plants and new developments in high temperature thermal energy storage technologies, Renew. Sustain. Energy Rev. 53 (2016) 1411–1432.
- [5] J. Serp, M. Allibert, O. Beneš, S. Delpech, O. Feynberg, V. Ghetta, D. Heuer, D. Holcomb, V. Ignatiev, J.L. Kloosterman, L. Luzzi, E. Merle-Lucotte, J. Uhlir, R. Yoshioka, D. Zhimin, The molten salt reactor (MSR) in generation IV: overview and perspectives, Prog. Nucl. Energy 77 (2014) 308–319.
- [6] S. Guo, J. Zhang, W. Wu, W. Zhou, Corrosion in the molten fluoride and chloride salts and materials development for nuclear applications, Prog. Mater. Sci. 97 (2018) 448–487.
- [7] J. Qiu, B. Leng, H. Liu, D.D. Macdonald, A. Wu, Y. Jia, W. Xue, G. Yu, X. Zhou, Effect of SO_4^{2-} on the corrosion of 316L stainless steel in molten FLiNaK salt, Corros. Sci. 144 (2018) 224–229.
- [8] Y.L. Wang, Q. Wang, H.J. Liu, C.L. Zeng, Effects of the oxidants H_2O and CrF_3 on the corrosion of pure metals in molten (Li,Na,K)F, Corros. Sci. 103 (2016) 268–282.
- [9] F.-Y. Ouyang, C.-H. Chang, B.-C. You, J.-J. Kai, Effect of moisture on corrosion of Ni-based alloys in molten alkali fluoride FLiNaK salt environments, J. Nucl. Mater. 437 (2013) 201–207.
- [10] G. Zong, Z.-B. Zhang, J.-H. Sun, J.-C. Xiao, Preparation of high-purity molten FLiNaK salt by the hydrofluorination process, J. Fluor. Chem. 197 (2017) 134–141.
- [11] B.C. Kelleher, K.P. Dolan, P. Brooks, M. Anderson, K. Sridharan, Batch scale hydrofluorination of Li_2BeF_4 to support molten salt reactor development, J. Nucl. Eng. Radiat. Sci. 35 (2015) 756–766.
- [12] J.H. Shaffer, Preparation and Handling of Salt Mixtures for the Molten Salt Reactor Experiment, ORNL-4616, (1971) 1–41.
- [13] W. Xue, X. Yang, J. Qiu, H. Liu, B. Zhao, H. Xia, X. Zhou, P. Huai, H. Liu, J. Wang, Effects of Cl^{3+} on the corrosion of SiC in LiF - NaF - KF molten salt, Corros. Sci. 114 (2017) 96–101.
- [14] H. Peng, M. Shen, C.Y. Wang, T. Su, Y. Zuo, L. Xie, Electrochemical investigation of the stable chromium species in molten FLINAK, RSC Adv. 5 (2015) 76689–76695.
- [15] H. De Van, Effect of Alloying Additions on Corrosion Behavior of Nickel-Molybdenum Alloys in Fused Fluoride Mixtures, ORNL-TM-2021, (1969) 1–51.
- [16] L.S. Richardson, D.C. Vreeland, W.D. Manly, Corrosion by Molten Fluorides, ORNL-1491, (1952) 1–19.
- [17] J.W. Koger, Effect of Fe Addition on Mass Transfer in a Hastelloy N - LiF-BeF₂-UF₄ Thermal Convection Loop System, ORNL-TM -4188, (1972) 1–28.
- [18] V. Pavlik, M. Konrik, M. Boca, Corrosion behavior of Incoloy 800H/HT in the fluoride molten salt FLiNaK + MFx (MFx = CrF₃, FeF₂, FeF₃ and NiF₂), N. J. Chem. 39 (2015) 9841–9847.
- [19] X.-X. Ye, H. Ai, Z. Guo, H. Huang, L. Jiang, J. Wang, Z. Li, X. Zhou, The high-temperature corrosion of Hastelloy N alloy (UNS N10003) in molten fluoride salts analysed by STXM, XAS, XRD, SEM, EPMA, TEM/EDS, Corros. Sci. 106 (2016) 249–259.
- [20] L.I. Katzin, E. Gebert Absorption Spectrum of Ferric Sulfate Complex ANL-4457, 5 (1950) 1–10.
- [21] F.H. Getman, A further study of the absorption spectra of potassium ferro- and ferricyanides, J. Phys. Chem. B 32 (1928) 187–191.

- [22] G. Harrington, B.R. Sundheim, Absorption spectra in molten salts, *Ann. N. Y. Acad. Sci.* 79 (1960) 950–970.
- [23] J.P. Young, Absorption spectra of several 3d transition metal ions in molten fluoride solution, *Inorg. Chem.* 8 (1969) 825–827.
- [24] Y. Zhu, J. Hou, G. Yu, J. Qiu, S. Chen, X. Zhou, Effects of exposing temperature on corrosion performance of weld joint of a Ni–Mo–Cr alloy, *J. Fluor. Chem.* 182 (2016) 69–75.
- [25] Y. Liu, Y. Song, H. Ai, M. Shen, H. Liu, S. Zhao, Y. Liu, Z. Fei, X. Fu, J. Cheng, Corrosion of Cr in molten salts with different fluoroacidity in the presence of CrF_3 , *Corros. Sci.* 169 (2020), 108636.
- [26] H. Ai, M. Shen, H. Sun, K.P. Dolan, C. Wang, M. Ge, H. Yin, X. Li, H. Peng, N. Li, L. Xie, Effects of O^{2-} additive on corrosion behavior of Fe–Cr–Ni alloy in molten fluoride salts, *Corros. Sci.* 150 (2019) 175–182.
- [27] H. Qiao, T. Nohira, Y. Ito, Electrochemical formation of Au_2Na alloy and the characteristics of $(\text{Au}_2\text{Na})^{\text{Au}}$ reference electrode in a LiF-NaF-KF eutectic melt, *Electrochim. Acta* 47 (2002) 4543–4549.
- [28] J. Hou, G. Yu, C. Zeng, H. Ai, R. Xie, Y. Chen, X. Zhou, L. Xie, J. Wang, Effects of exposing duration on corrosion performance in weld joint of Ni–Mo–Cr alloy in FLiNaK molten salt, *J. Fluor. Chem.* 191 (2016) 110–119.
- [29] F.-Y. Ouyang, C.-H. Chang, J.-J. Kai, Long-term corrosion behaviors of Hastelloy-N and Hastelloy-B3 in moisture-containing molten FLiNaK salt environments, *J. Nucl. Mater.* 446 (2014) 81–89.
- [30] H. Ai, S. Liu, X.-X. Ye, L. Jiang, B. Zhou, X. Yang, B. Leng, Z. Li, Metallic impurities induced corrosion of a $\text{Ni}^{+26}\text{W}^{-6}\text{Cr}$ alloy in molten fluoride salts at 850 °C, *Corros. Sci.* 178 (2021), 109079.
- [31] H. Ai, J. Hou, X.-X. Ye, C.L. Zeng, H. Sun, X. Li, G. Yu, X. Zhou, J.-Q. Wang, Influence of graphite-alloy interactions on corrosion of Ni–Mo–Cr alloy in molten fluorides, *J. Nucl. Mater.* 503 (2018) 116–123.
- [32] Y. Zhu, J. Qiu, J. Hou, W. Liu, H. Chen, H. Ai, G. Yu, J. Wang, X. Zhou, Effects of SO_4^{2-} ions on the corrosion of GH3535 weld joint in FLiNaK molten salt, *J. Nucl. Mater.* 492 (2017) 122–127.
- [33] D.F. Williams, L.M. Toth, E.D. Collins, The influence of Lewis acid/base chemistry on the removal of gallium by volatility from weapons-grade plutonium dissolved in molten chlorides, *Nucl. Technol.* 136 (2017) 367–370.
- [34] L.C. Olson, Materials Corrosion in Molten LiF-NaF-KF Eutectic Salt, University of Wisconsin-Madison, 2009.
- [35] M.N. Berberan Santos, Beer's Law revisited, *J. Chem. Educ.* 67 (1990) 168–170.
- [36] J.E. McMurry, R.C. Fay, S. Dillon, Laboratory Manual for General Chemistry, (2013).
- [37] D.I. Sorokin, N.L. Sidorov, I.M. Nikitin, Mass-spectrometric determination of the enthalpies of dissociation of gaseous complex fluorides into neutral and charged species. V. heats of formation of FeF_3^- and FeF_4^- , *International Journal of Mass Spectrometry & Ion Physics*, (1981).
- [38] C.A. Zarzana, G.S. Groenewold, M.T. Benson, J. Delmore, Iron fluoroanions and their clusters by electrospray ionization of a fluorinating ionic liquid, *J. Am. Soc. Mass Spectrom.* 26 (2015) 1559–1569.
- [39] J.W. Koger, Corrosion and mass transfer characteristics of $\text{NaBF}_4\text{-NaF}$ (92–8 mole %) in Hastelloy N, ORNL-TM-3866, (1972) 1–88.
- [40] I.N. Ozeryanaya, Corrosion of metals by molten salts in heat-treatment processes, *Met. Sci. Heat. Treat.* 27 (1985) 184–188.
- [41] W.H. Jordan, S.J. Croner, A.J. Miller Aircraft nuclear propulsion project quarterly progress report, 4 (1958) 117–142.
- [42] D.L. Manning, G. Mamantov, Electrochemical studies of oxide ions and related species in molten fluorides, *Chem. Inform.* 8 (1977) 480–483.
- [43] M. Shen, H. Peng, M. Ge, Y. Zuo, L. Xie, Use of square wave voltammeter for online monitoring of O^{2-} concentration in molten fluorides at 600 °C, *J. Electroanal. Chem.* 748 (2015) 34–39.
- [44] C.F. Baes, The chemistry and thermodynamics of molten salt reactor fuels, *J. Nucl. Mater.* 51 (1974) 149–162.
- [45] G. Duran, D. Rodrigues, S. Delpech, Dynamic reference electrode development for redox potential measurements in fluoride molten salt at high temperature, *Electrochim. Acta* 195 (2016) 19–26.
- [46] H. Ai, X.-X. Ye, L. Jiang, B. Leng, M. Shen, Z. Li, Y. Jia, J.-Q. Wang, X. Zhou, Y. Xie, L. Xie, On the possibility of severe corrosion of a Ni–W–Cr alloy in fluoride molten salts at high temperature, *Corros. Sci.* 149 (2019) 218–225.
- [47] W.-J.C. Robert, S. Sellers, Brian C. Kelleher, Mark H. Anderson, Kumar Sridharan, Chaur-Jeng Wang, Todd R. Allen, Corrosion of 316L stainless steel alloy and Hastelloy-N superalloy in molten eutectic LiF-NaF-KF salt and interaction with graphite, *Nucl. Technol.* (2014) 192–199.
- [48] L.C. Olson, J.W. Ambrosek, K. Sridharan, M.H. Anderson, T.R. Allen, Materials corrosion in molten LiF-NaF-KF salt, *J. Fluor. Chem.* 130 (2009) 67–73.
- [49] J. Qiu, Y. Zou, Z. Li, H. Xu, Corrosion behaviors of nickel-based high temperature alloys in molten FLiNaK salt, *Nucl. Tech.* 38 (2015) 55–60.
- [50] F.-Y. Ouyang, C.-H. Chang, J.-J. Kai, Long-term corrosion behaviors of Hastelloy-N and Hastelloy-B3 in moisture-containing molten FLiNaK salt environments, *J. Nucl. Mater.* 446 (2014) 81–89.
- [51] H.O. Nam, A. Bengtson, K. Vörtler, S. Saha, R. Sakidja, D. Morgan, First-principles molecular dynamics modeling of the molten fluoride salt with Cr solute, *J. Nucl. Mater.* 449 (2014) 148–157.